Supporting Information:

Peptide-Directed PdAu Nanoscale Phase Separation: Toward Controlled Bimetallic Architecture for Catalytic Materials

Nicholas M. Bedford,[1*] Allison R. Showalter,[2] Taylor J. Woehl,[1] Zak E. Hughes,[3] Sungsik Lee,[4] Benjamin Reinhart,[4] S. Piril Ertem,[5] E. Bryan Coughlin,[5] Yang Ren,[4] Tiffany R. Walsh,[3] Bruce A. Bunker[2]

[1] *Applied Chemical and Materials Division, National Institute of Standards and Technology, Boulder, CO 80305 USA*

[2] *Department of Physics, University of Notre Dame, Notre Dame, IN 46556 USA*

[3] *Institute for Frontier Materials, Deakin University, Geelong, Vic. 3216 Australia*

[4] *X-ray Sciences Division, Argonne National Laboratory, Argonne, IL 60439 USA*

[5] *Department of Polymer Science and Engineering, University of Massachusetts Amherst, Amherst, MA, 01003 USA*

Contents

Figure S11: Total structure functions for the peptide-capped PdAu bimetallic nanoparticles.

Figure S12: Atomic PDFs for peptide-capped PdAu bimetallic, monometallic Pd and Au nanoparticles to 10 Å.

Figure S13: Atomic PDFs for peptide-capped PdAu bimetallic, monometallic Pd and Au nanoparticles to 40 Å.

Figure S15: Cross-sections of RMC-generated configurations for peptide-capped PdAu bimetallic nanoparticles.

Figure S15: Atomic PDFs, calculated as $g(r) = \rho(r)/\rho_0$, of the surface atoms calculated from the RMC-generated bimetallic nanoparticle configurations for a) 3:1 Pd:Au nanoparticles, b) 1:1 Pd:Au bimetallic nanoparticles, and c) 1:3 Pd:Au bimetallic nanoparticles.

Figure S16: Representative snapshots of the adsorbed peptides taken from the REST-MD simulations.

Figure S17: Distribution of tilt angle of Trp, Arg and His residues with metal surfaces calculated from the REST-MD simulations.

Figure S18: CVs of peptide-capped monometallic Pd and Au nanoparticles in 1.0 M NaOH, 1.0 M methanol.

Figure S19: CVs of commercially available Pd/C in 1.0 M NaOH, 1.0 M methanol.

Section S1: Ionomer Synthesis

Materials

Isoprene (99%, Alfa Aesar) was distilled prior to use and stored under nitrogen. 4-vinylbenzyl chloride (VBCl) (90%, Acros Organics) was passed through a column of basic alumina. 3,7-Dioxa-4-aza-6-phosphanonanoic acid, 4,5-bis (1,1-dimethylethyl)-6-ethoxy-2,2-dimethyl-6-oxide (SG1) (BlockBuilder™) was kindly provided by Arkema.

Polymerization procedure for polyisoprene-*ran*-poly(vinylbenzyl chloride) (PI-*ran*-PVBCl) copolymer

The synthesis of PI-*ran*-PVBCl copolymers were performed following a previously reported procedure.[1, 2] Isoprene (24 ml, 240 mmol), vinylbenzyl chloride (VBCl) (11.6 ml, 82.3 mmol) and SG1 (41 mg, 106 μmol) were transfered into a Teflon® sealed Schlenk flask equipped with a magnetic stirrer. The reaction flask was degassed by three freeze-pump-thaw cycles, and subsequently was refilled with nitrogen gas. The copolymerization reaction was performed at 125 ^{o}C for 19 h. The reaction was quenched by cooling the flask in an ice bath. The viscous reaction mixture was diluted with dichloromethane, and then precipitated into excess methanol to recover the copolymer as a colorless solid (7.5g, 25% yield, M_n=38000 g/mol as determined by GPC against polystyrene standards with THF as solvent). Copolymer ratio was determined *via* ^{1}H NMR and was found to be 24.9% VBCl to 75.1% isoprene (Figure S16).

General procedure for quaternization

Quaternization of PI-*ran*-PVBCl precursor into PI-*ran*-P[VBTMA][Cl] was described in detail previously.[1, 2] Approximately 1 gram of precursor copolymer was weighed in a 20 mL syntillation vial. About 15 mL 50 wt% aqueous trimethylamine solution was added. The top of the vial was covered with Teflon tape and sealed tightly. The vial was further wrapped with parafilm. The reaction mixture was heated to 60 °C overnight. During the reaction PI-*ran*-PVBCl copolymer dissolved in the aqueous reaction mixture. After the reaction the vial was cooled down, water was removed first under constant airflow, and subsequently under reduced pressure at 40 °C overnight to obtain the quaternized polymer polyisoprene-ran-poly(vinyl benzyl trimethylammonium chloride) (PI-*ran*-P[VBTMA][Cl]) as a pale yellow solid. Quantitative conversion of benzyl chloride units into BTMA salts was confirmed through FTIR spectroscopy by observing the complete disappearance of the C-Cl stretching band at 674 cm^{-1} and C-H wagging band at 1265 cm^{-1} of the chloromethyl group after quaternization. Ion exchange capacity (IEC) of PI-*ran*-P[VBTMA][Cl] was calculated from the ratio of VBCl to isoprene determined by ^{1}H NMR spectroscopy and was found as 2.4 mmol/g. Quaternized polymers were stored at -30 °C in the dark until used.

Section S2: Simulation Details

REST-MD Simulations

Replica exchange with solute tempering is molecular simulation technique that provides advanced sampling of the conformational space of a system. More information of the REST technique can be found elsewhere.[3-5] Unless otherwise specified the simulation details are as described in previous work.

Each system simulated consisted of a single peptide, a Au/Pd(111) *p*(20×24) supercell five atomic layers thick, 6605 water molecules and a appropriate number of Cl^- counter ions to ensure the overall charge neutrality of the system. The peptides were simulated in their zwitterionic forms and with each residue assigned their likely protonation state at pH 7. The separation between the metal slab and its periodic image was greater than 55 Å, with the water density in the centre of the system equal to that of bulk water at ambient temperature and pressure.

The CHARMM22* FF[6, 7] and the modified version of the TIP3P water model were used to model the peptide chain and water molecules respectively. The interactions between the metal slabs and the other species were described through the use a modified version of the CHARMM-METAL FF.[8, 9] The CHARMM-METAL FF was modified by scaling the hetro-atomic Lennard-Jones ε parameter for all M-X interactions by $1\sqrt{6}$, where M is metal atom and X is any non-metal atom. The ε parameter for the Au-Au and Pd-Pd self-interaction was not scaled in order to ensure that the behaviour of the bulk metal is preserved. Further details on the modification of the FF are described elsewhere.[9]

All simulations were performed using GROMACS version 5.0.[10] The simulations were performed in the Canonical (*NVT*) ensemble, at 300 K with the Nosé-Hoover thermostat[11, 12] used to regulate the temperature. The cutoff for the LJ non-bonded interactions was 11 Å, with the force switched smoothly to zero from 10 Å. The electrostatic interactions were calculated using a particle mesh Ewald (PME)[13] summation with a real-space cutoff of 11 Å. Each system simulated consisted of 16 replicas spanning an "effective temperature" window of 300-500 K. The initial peptide conformation in each replica differed, such that a wide range of secondary structures were present. Each replica was equilibrated at its "effective temperature" for 0.5 ns, during which time no exchanges between replicas were attempted. Following this a production run of 20×10^6 MD steps was performed, with a exchanges between adjacent replicas attempted every 1000 steps. A timestep of 1 fs was used for all simulations and coordinates written out every 1000 steps.

Analysis of Simulation Trajectories

All analysis of the simulation trajectories was carried out over the full 20,000 frames of the baseline trajectory (*i.e.* replica corresponding to λ=0/T=300 K).

The degree of contact between and residue and the metal surface was determined by calculating the fraction of the trajectory that a reference site within the side-chain of each residue was within a cutoff distance of the metal surface. The reference sites and cutoff distances have been given in previous work.[5, 9]

A cluster analysis of the baseline trajectory was performed in order to identify distinct adsorbed conformations of the peptides with their Boltzmann-weighted populations. The Daura clustering algorithm[14] was applied over the backbone atoms of the peptide, the RMSD cutoff was 2.0 Å for AuBP1/Pd4 and 2.2 Å for H1, ensuring that the cutoff was the constant with respect to the length of the peptide.

Table S1: Sizing and aspect ratio analysis from TEM images for peptide-capped bimetallic nanoparticles. Note that the similarities of aspect ratios suggest any observed anisotropic features are likely due to STEM drift.

Sample	Average Size (TEM)	Aspect Ratio (TEM)
AuBP1 – 3:1 Pd:Au	2.04 ± 0.71 nm	1.20 ± 0.12
AuBP1 – 1:1 Pd:Au	2.06 ± 0.35 nm	1.23 ± 0.13
AuBP1 – 1:3 Pd:Au	1.98 ± 0.31 nm	1.27 ± 0.13
H1 – 3:1 Pd:Au	2.08 ± 0.36 nm	1.22 ± 0.13
H1 – 1:1 Pd:Au	2.00 ± 0.32 nm	1.27 ± 0.13
H1 – 1:3 Pd:Au	2.01 ± 0.32 nm	1.30 ± 0.13
Pd4 – 3:1 Pd:Au	2.08 ± 0.89 nm	1.27 ± 0.13
Pd4 – 1:1 Pd:Au	1.97 ± 0.80 nm	1.27 ± 0.13
Pd4 – 1:3 Pd:Au	2.02 ± 0.34 nm	1.28 ± 0.12

Table S2: Bimetallic XAFS Debye-Waller factors for each peptide-capped nanoparticle as determined from EXAFS modeling. For monometallic Pd, Pd-Cl contributions were used in the modeling and are highlighted.

Catalyst	Pd-Pd Debye-Waller factor	Pd-Au Debye-Waller factor	Au-Pd Debye-Waller factor	Au-Au Debye-Waller factor
AuBP1		Pd-Cl Debye-Waller factor		
Pd	0.008 ± 0.003	0.01 ± 0.01		
3:1 Pd:Au	0.010 ± 0.004	0.013 ± 0.02	0.006 ± 0.002	0.02 ± 0.01
1:1 Pd:Au	0.001 ± 0.005	0.001 ± 0.003	0.006 ± 0.003	0.007 ± 0.002
1:3 Pd:Au	0.002 ± 0.004	0.004 ± 0.02	0.007 ± 0.006	0.010 ± 0.004
Au	-	-	-	0.0074 ± 0.0005
H1		Pd-Cl Debye-Waller factor		
Pd	0.007 ± 0.002	0.01 ± 0.02		
3:1 Pd:Au	0.003 ± 0.005	0.01 ± 0.02	0.008 ± 0.001	0.02 ± 0.01
1:1 Pd:Au	0.003 ± 0.001	0.005 ± 0.002	0.012 ± 0.004	0.009 ± 0.004
1:3 Pd:Au	0.002 ± 0.004	0.02 ± 0.01	0.005 ± 0.008	0.005 ± 0.004
Au	-	-	-	0.009 ± 0.001
Pd4		Pd-Cl Debye-Waller factor		
Pd	0.007 ± 0.003	0.01 ± 0.01		
3:1 Pd:Au	0.02 ± 0.02	0.001 ± 0.002	0.004 ± 0.004	0.007 ± 0.003
1:1 Pd:Au	0.004 ± 0.001	0.006 ± 0.002	0.006 ± 0.002	0.006 ± 0.001
1:3 Pd:Au	0.001 ± 0.009	0.011 ± 0.005	0.011 ± 0.005	0.008 ± 0.003
Au	-	-	-	0.0071 ± 0.0005

Table S3: Percentage of trajectory that the contact site of each residue is in direct contact with the Au(111) or Pd(111) surface. Residues that in are in direct contact with the surface for 75%+ are highlighted.

AuBP1			Pd4			H1		
Residue	Au	Pd	Residue	Au	Pd	Residue	Au	Pd
W	86	94				W	96	90
A	79	57	T	24	32	A	68	42
G	90	92	S	33	53	G	85	73
A	57	81	N	83	76	A	74	60
K	48	55	A	67	46	K	40	42
R	95	96	V	71	69	R	82	90
L	77	57	H	62	69	H	77	54
V	66	77	P	10	42	P	28	52
L	63	90	T	39	27	T	37	60
R	98	98	L	38	73	L	86	87
R	99	98	R	89	98	R	98	98
E	39	35	H	73	56	H	50	52
			L	47	52	L	69	83

Table S4: Percentage population of top ten most populous clusters, the total number of clusters and the conformational entropy of each peptide adsorbed at the aqueous Au(111) and Pd(111) surfaces.

	AuBP1		Pd4		H1	
Cluster Rank	Au	Pd	Au	Pd	Au	Pd
1	33.5	31.5	25.9	17.0	29.2	26.4
2	22.6	21.3	9.2	12.3	19.1	20.0
3	13.6	10.6	7.5	11.3	12.0	13.4
4	5.7	9.8	7.3	10.1	8.7	11.3
5	4.3	8.0	5.8	7.7	7.5	6.9
6	2.9	3.6	5.3	7.3	3.3	3.0
7	2.5	3.0	4.5	7.1	2.8	2.8
8	2.4	2.2	42	2.3	2.7	2.8
9	1.9	1.7	4.2	2.2	2.5	2.7
10	1.5	1.6	4.2	2.0	2.1	2.6
Total	52	40	83	76	52	54
S_{conf}	2.18	2.17	2.87	2.80	2.35	2.31

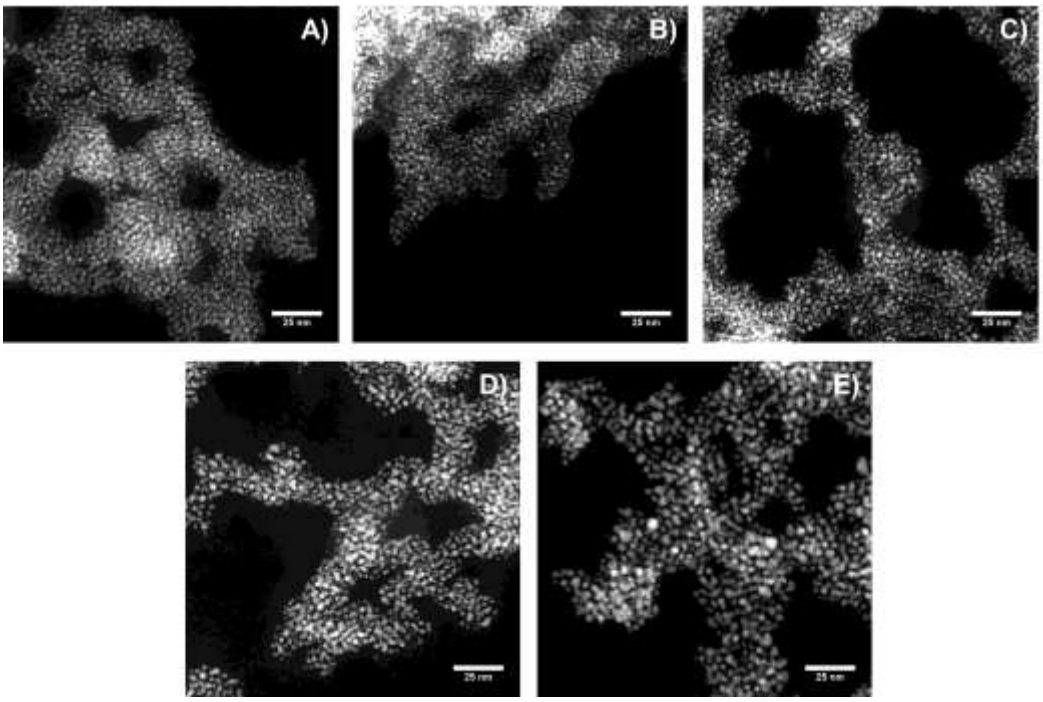

Figure S1. HRTEM of AuBP1-capped nanoparticles: a) 100% Pd, b) 3:1 Pd:Au, c) 1:1 Pd:Au, d) 1:3 Pd:Au, e) 100% Au

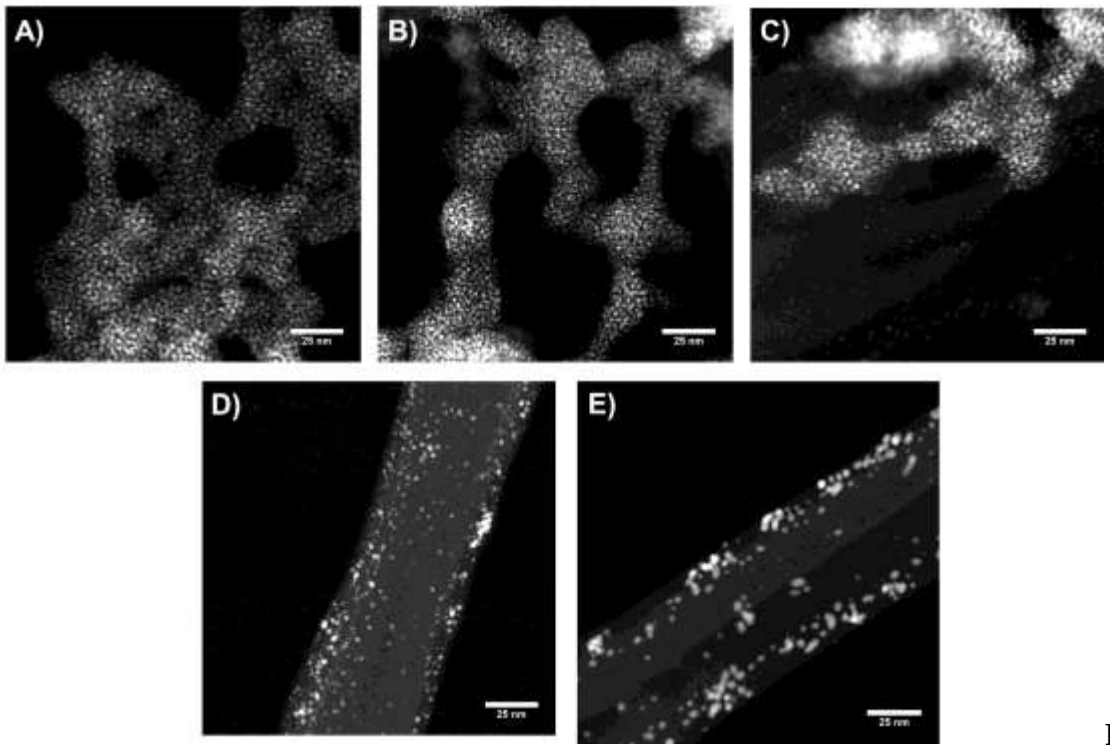

Figure S2. HRTEM of H1-capped nanoparticles: a) 100% Pd, b) 3:1 Pd:Au, c) 1:1 Pd:Au, d) 1:3 Pd:Au, e) 100% Au

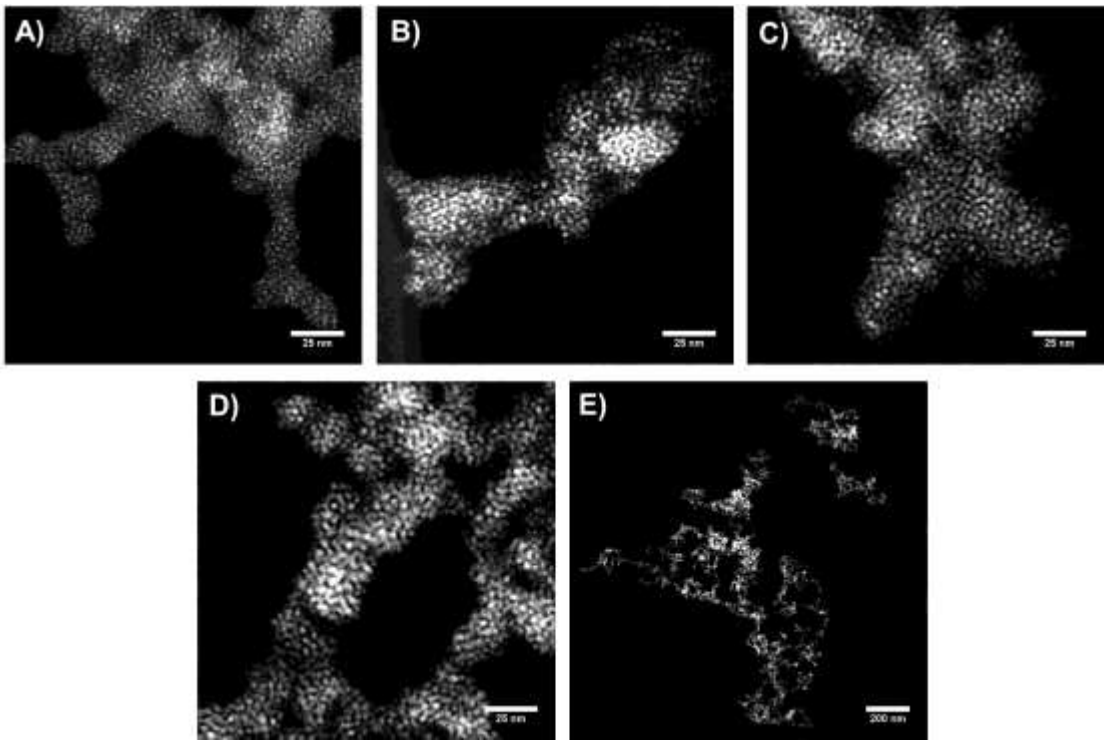

Figure S3. HRTEM of Pd4-capped nanoparticles: a) 100% Pd, b) 3:1 Pd:Au, c) 1:1 Pd:Au, d) 1:3 Pd:Au, e) 100% Au

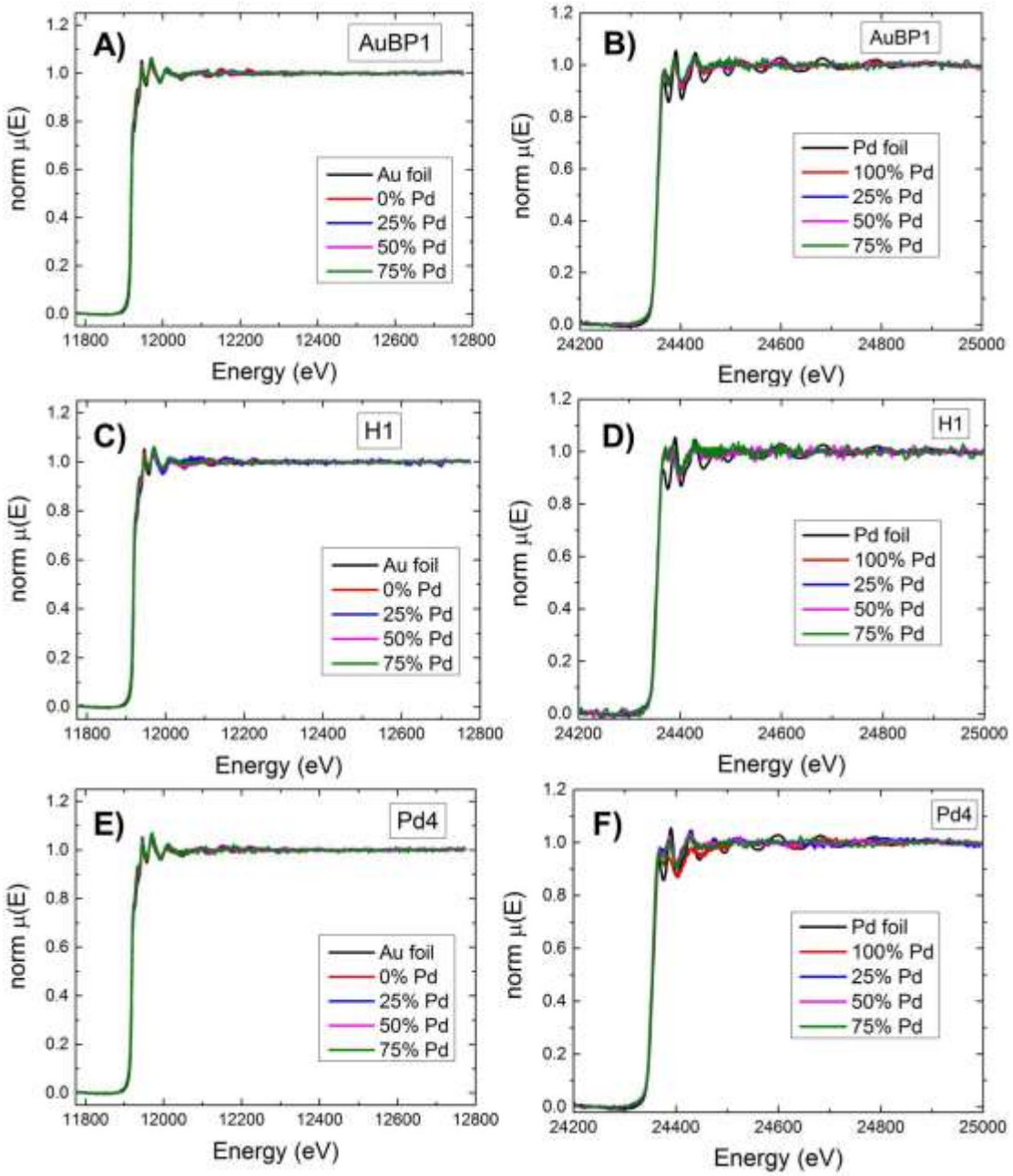

Figure S4. XAFS for a) AuBP1-capped nanoparticles around the Au L_3-edge; b) AuBP1-capped nanoparticles around the Pd K-edge; c) H1-capped nanoparticles around the Au L_3-edge; d) H1-capped nanoparticles around the Pd K-edge; e) Pd4-capped nanoparticles around the Au L_3-edge; and f) Pd4-capped nanoparticles around the Pd K-edge.

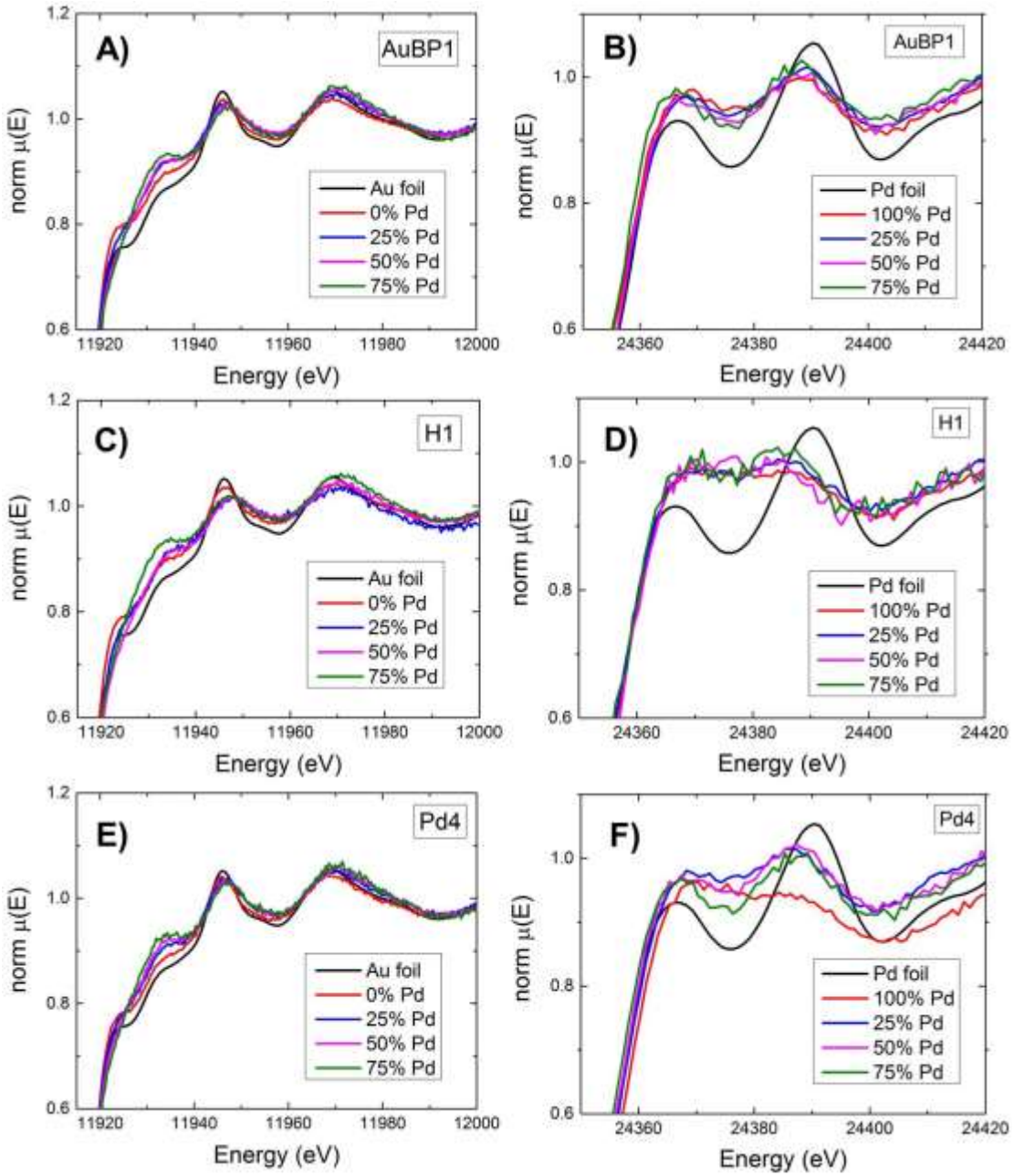

Figure S5. XANES for a) AuBP1-capped nanoparticles at the Au L_3-edge; b) AuBP1-capped nanoparticles at the Pd K-edge; c) H1-capped nanoparticles at the Au L_3-edge; d) H1-capped nanoparticles at the Pd K-edge; e) Pd4-capped nanoparticles at the Au L_3-edge; and f) Pd4-capped nanoparticles at the Pd K-edge.

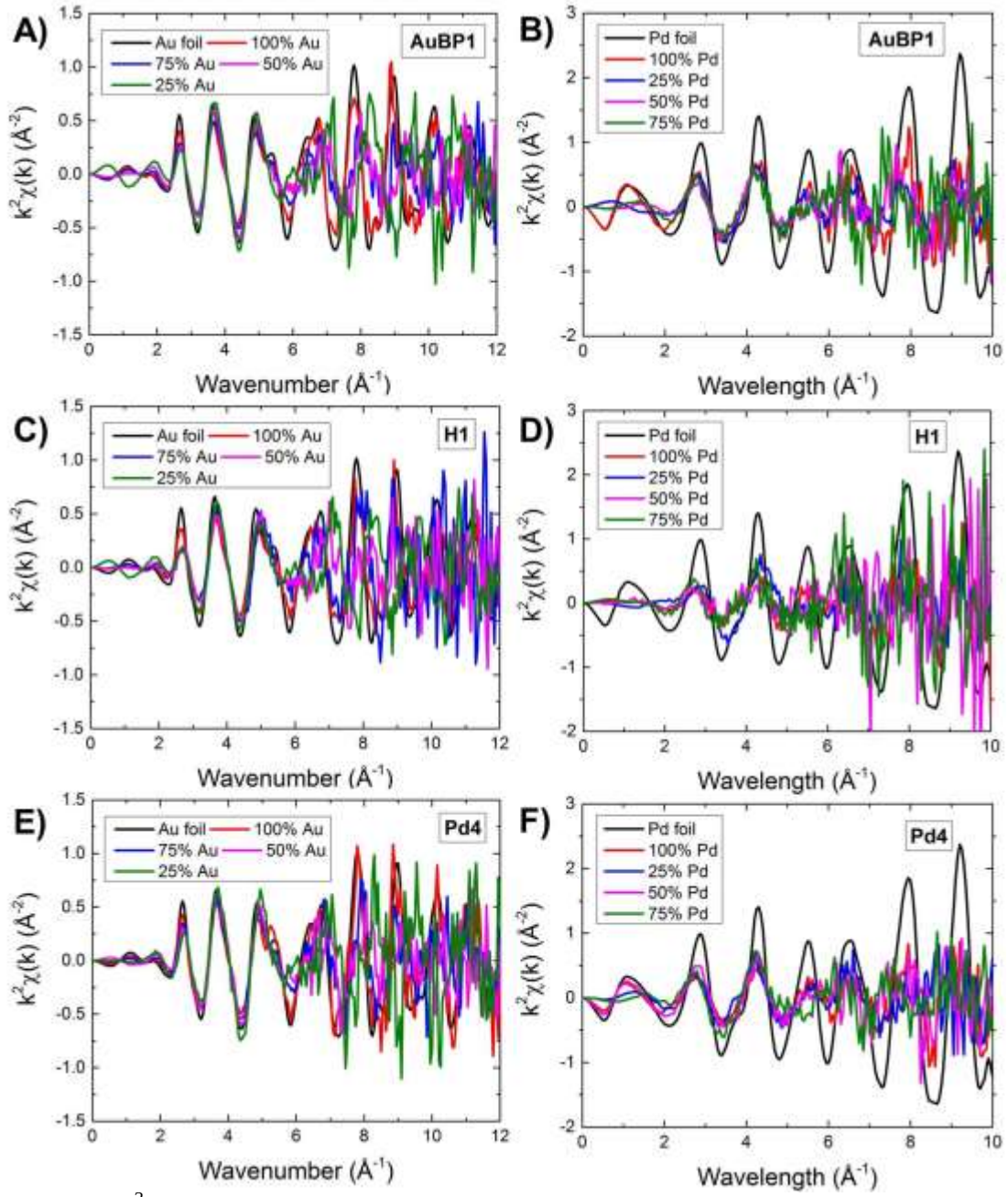

Figure S6. k^2-weighted EXAFS data a) AuBP1-capped nanoparticles around the Au L_3-edge; b) AuBP1-capped nanoparticles around the Pd K-edge; c) H1-capped nanoparticles around the Au L_3-edge; d) H1-capped nanoparticles around the Pd K-edge; e) Pd4-capped nanoparticles around the Au L_3-edge; and f) Pd4-capped nanoparticles around the Pd K-edge.

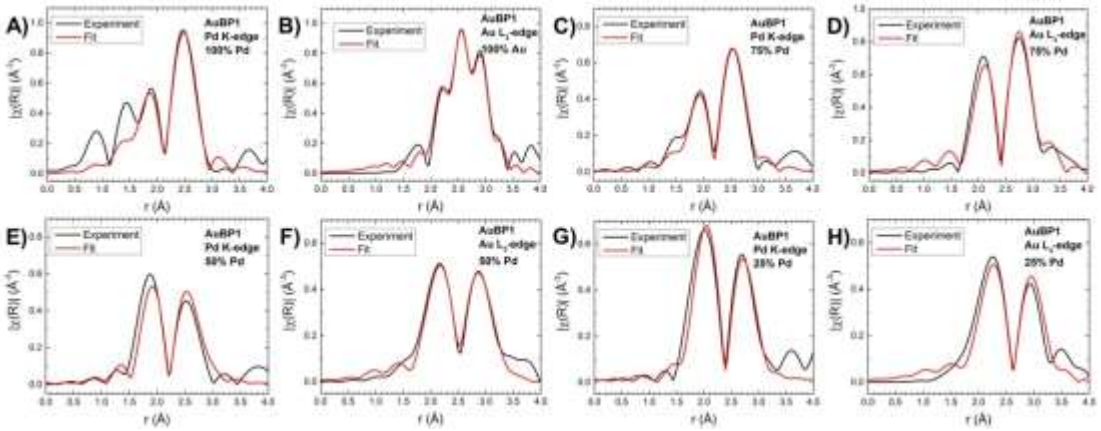

Figure S7. EXAFS fitting for AuBP1-capped nanoparticles: a) 100% Pd; b) 100% Au; c) 3:1 Pd:Au (Au L_3-edge); d) 3:1 Pd:Au (Pd K-edge); e) 1:1 Pd:Au (Au L_3-edge); f) 1:1 Pd:Au (Pd K-edge); g) 1:3 Pd:Au (Au L_3-edge); and h) 1:3 Pd:Au (Pd K-edge).

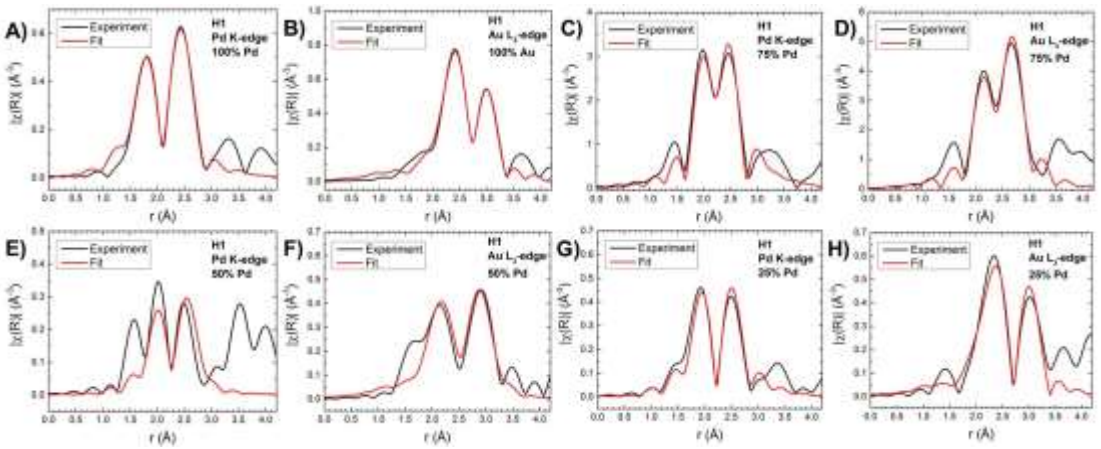

Figure S8. EXAFS fitting for H1-capped nanoparticles: a) 100% Pd; b) 100% Au; c) 3:1 Pd:Au (Au L_3-edge); d) 3:1 Pd:Au (Pd K-edge); e) 1:1 Pd:Au (Au L_3-edge); f) 1:1 Pd:Au (Pd K-edge); g) 1:3 Pd:Au (Au L_3-edge); and h) 1:3 Pd:Au (Pd K-edge).

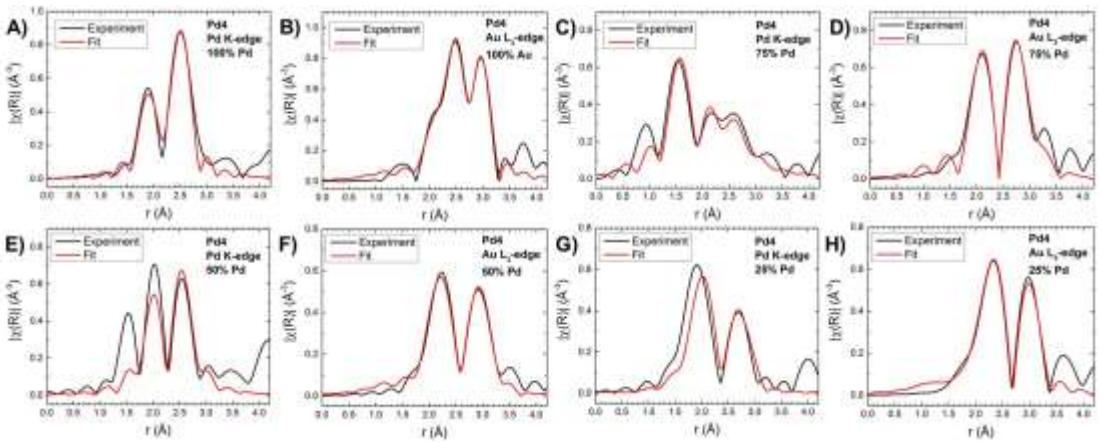

Figure S9. EXAFS fitting for Pd4-capped nanoparticles: a) 100% Pd; b) 100% Au; c) 3:1 Pd:Au (Au L_3-edge); d) 3:1 Pd:Au (Pd K-edge); e) 1:1 Pd:Au (Au L_3-edge); f) 1:1 Pd:Au (Pd K-edge); g) 1:3 Pd:Au (Au L_3-edge); and h) 1:3 Pd:Au (Pd K-edge).

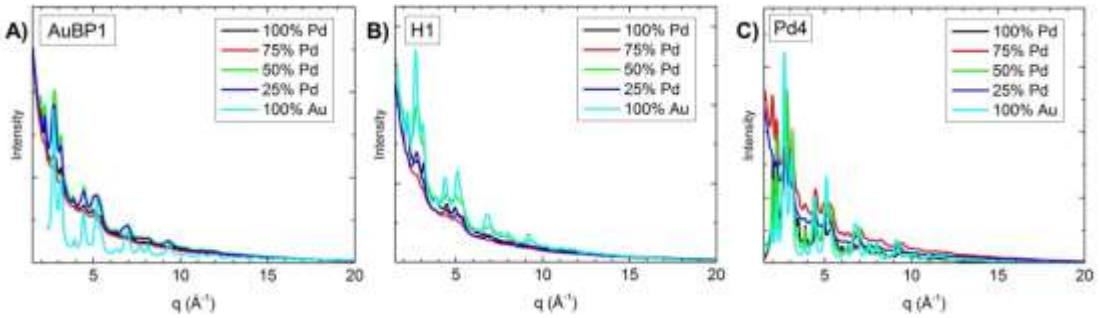

Figure S10. HE-XRD patterns from peptide-enabled bimetallic and monometallic nanoparticles with a) AuBP1; b) H1; and c) Pd4.

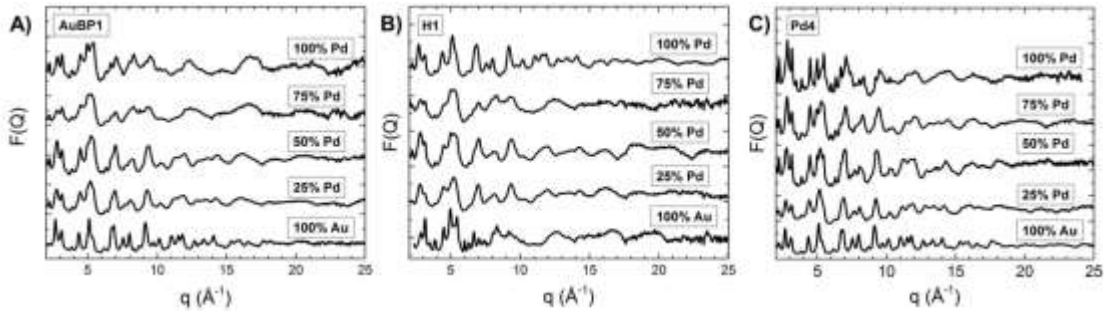

Figure S11. Total structure functions for peptide-enabled bimetallic and monometallic nanoparticles with a) AuBP1; b) H1; and c) Pd4.

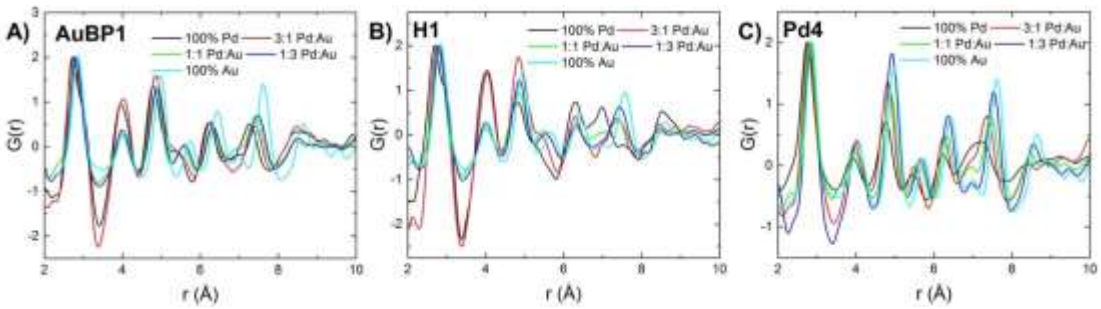

Figure S12. Atomic PDFs up to 10 Å for peptide-enabled bimetallic and monometallic nanoparticles with a) AuBP1; b) H1; and c) Pd4.

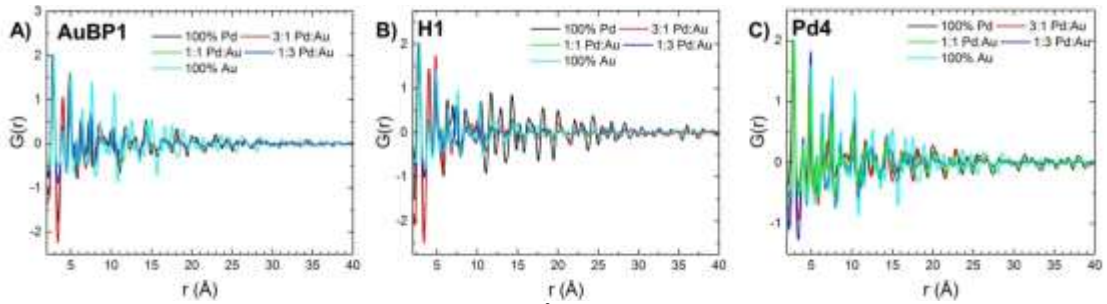

Figure S13. Atomic PDFs up to 40 Å for peptide-enabled bimetallic and monometallic nanoparticles with a) AuBP1; b) H1; and c) Pd4.

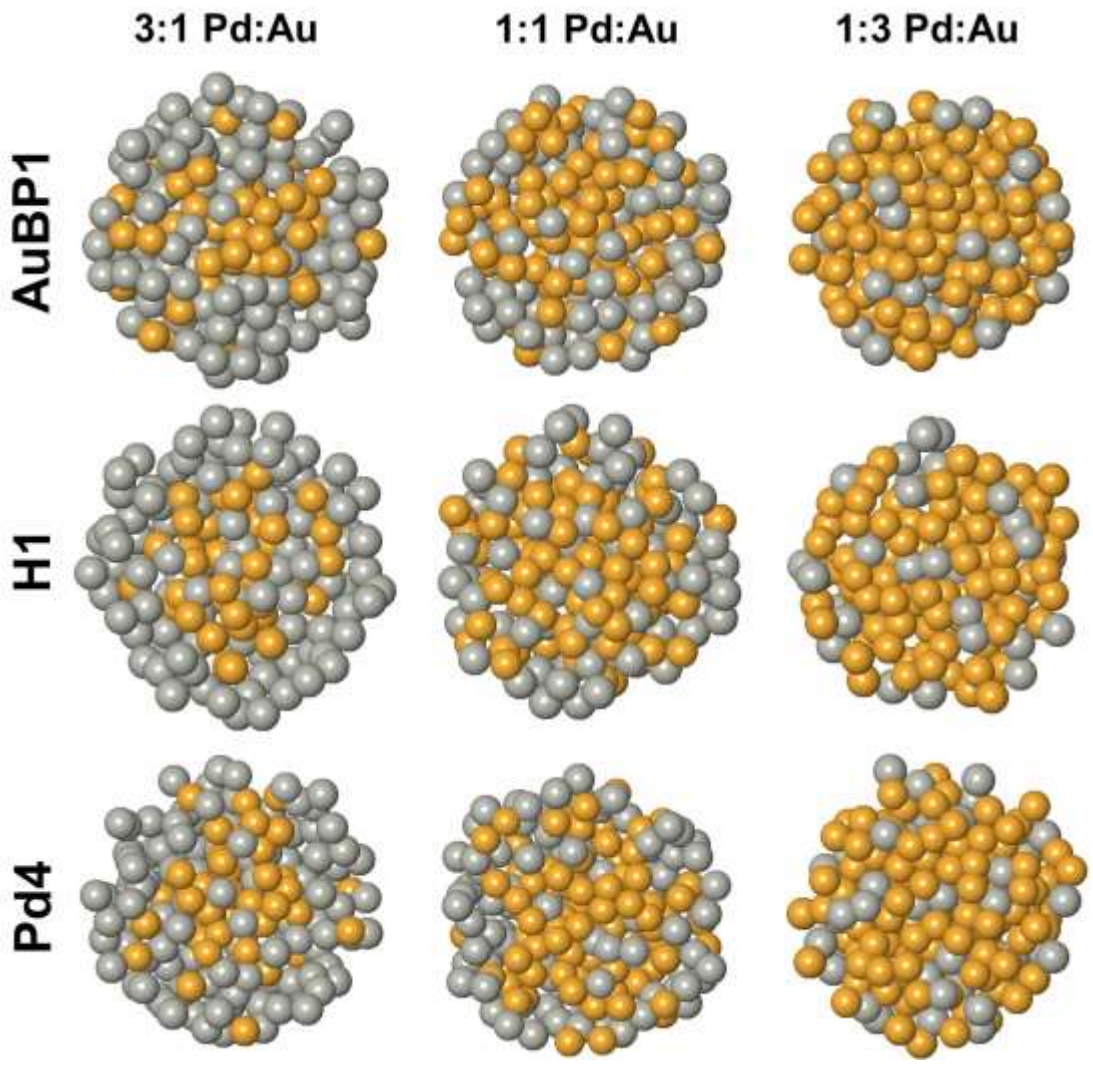

Figure S14. Cross sections of RMC generated configurations for peptide-capped PdAu bimetallic nanoparticles.

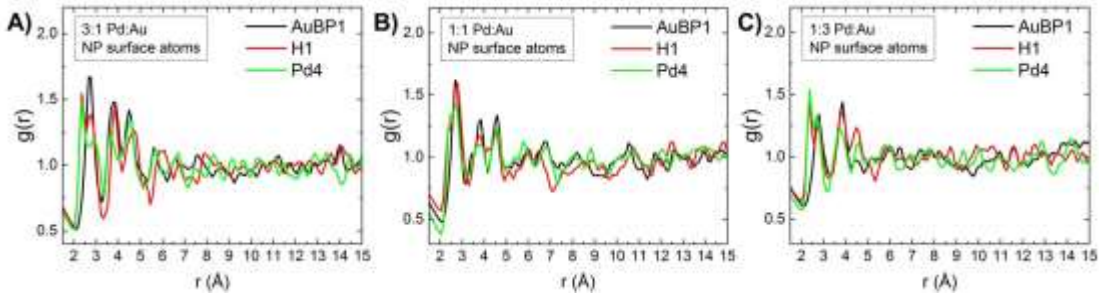

Figure S15: Atomic PDFs, calculated as $g(r) = \rho(r)/\rho_0$, of the surface atoms calculated from the RMC-generated bimetallic nanoparticle configurations for a) 3:1 Pd:Au nanoparticles, b) 1:1 Pd:Au bimetallic nanoparticles, and c) 1:3 Pd:Au bimetallic nanoparticles.

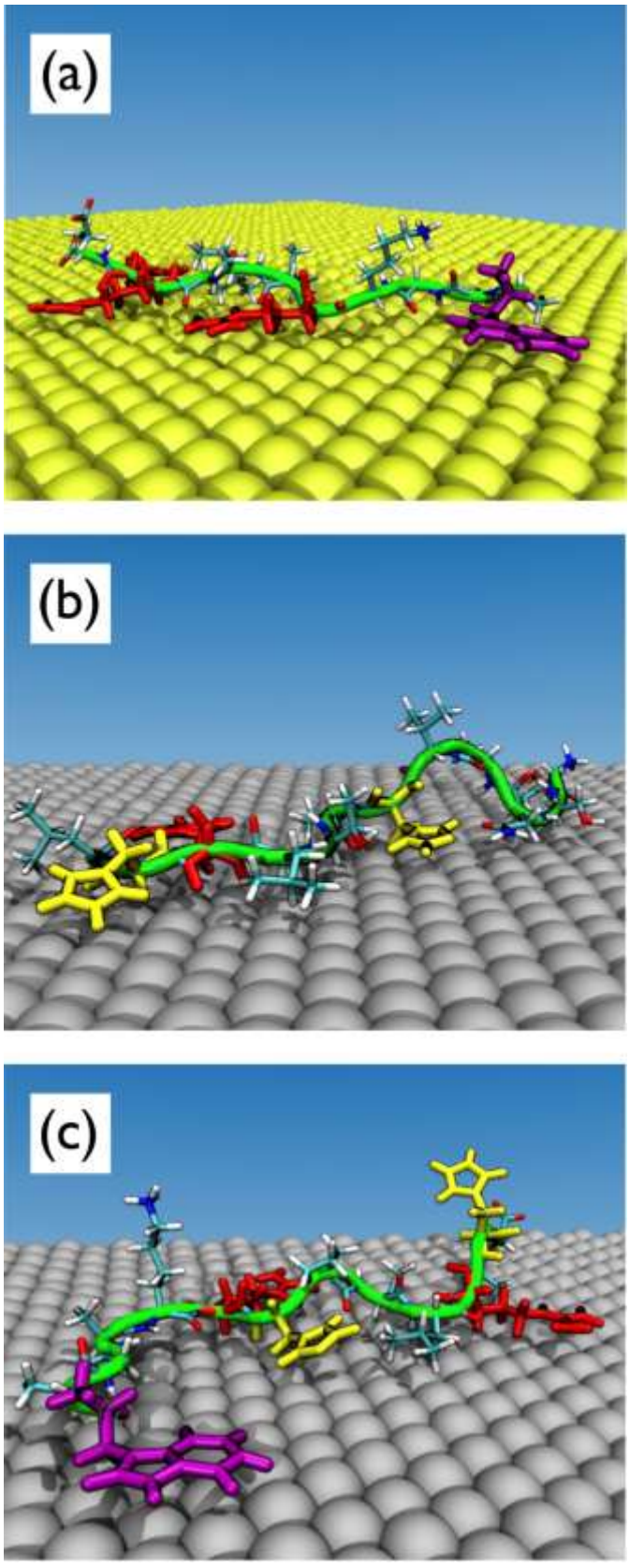
(a)
(b)
(c)

Figure S16. Representative snapshots taken from the REST-MS simulations of (a) AuBP1 on Au(111), (b) Pd4 on Pd(111) and (c) H1 on Pd(111). The peptide backbone is colored green, while the Arg, His and Trp residues are colored red, yellow and purple, respectively.

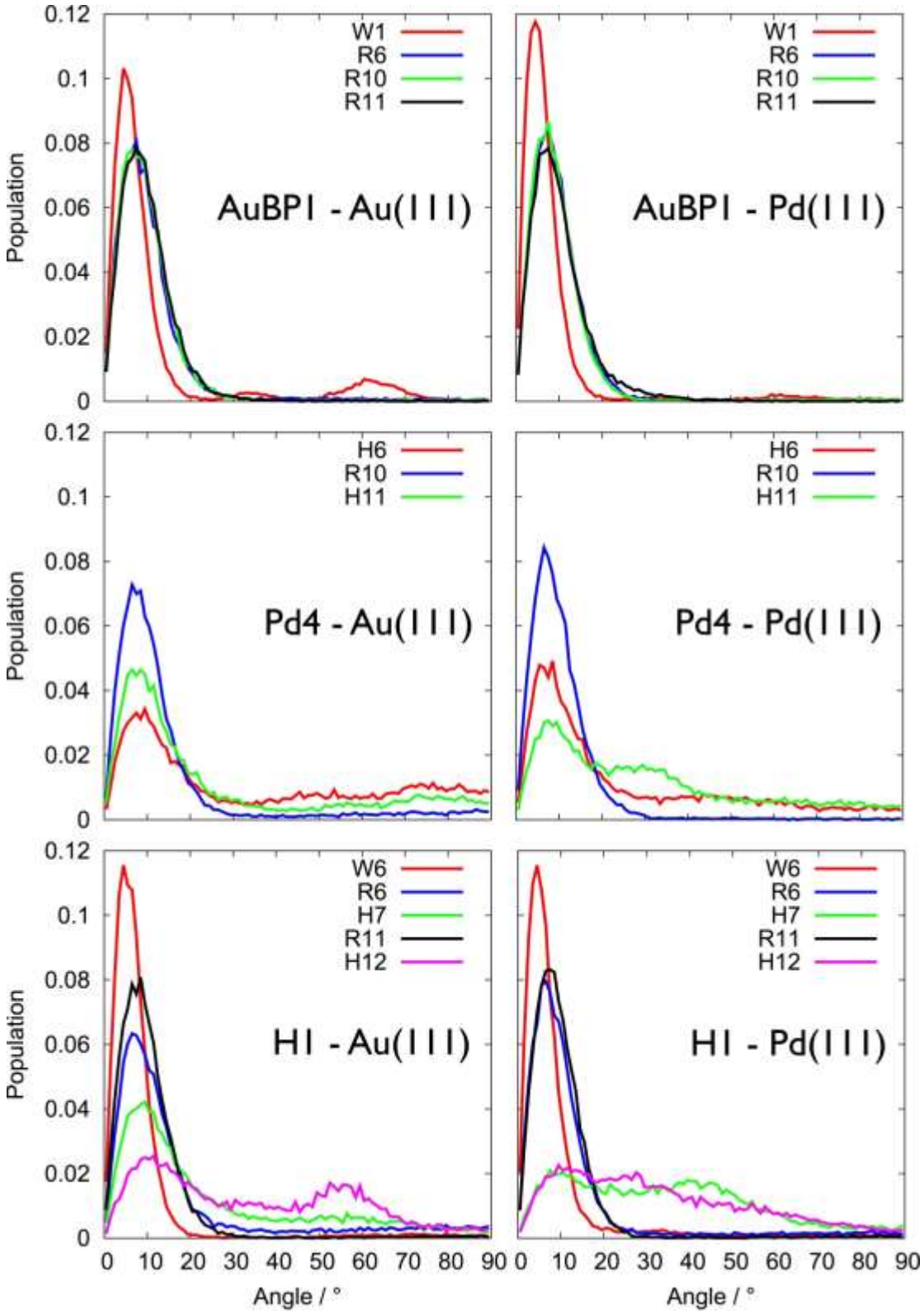

Figure S17. Population distributions of the angle between the plane of the aromatic rings or guanidinium group of the His, Trp and Arg residues of the peptides adsorbed at the aqueous Au/Pd(111) interfaces, obtained from the REST-MD simulations.

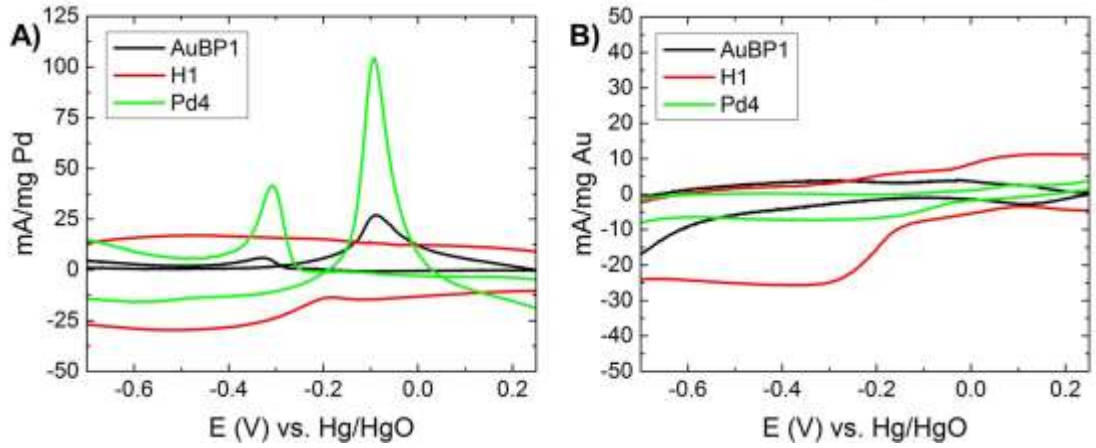

Figure S18. Background subtracted CVs of a) peptide-capped Pd nanoparticles and b) peptide-capped Au nanoparticles in 1.0 M NaOH, 1.0 M methanol cycled at 20 mV/s.

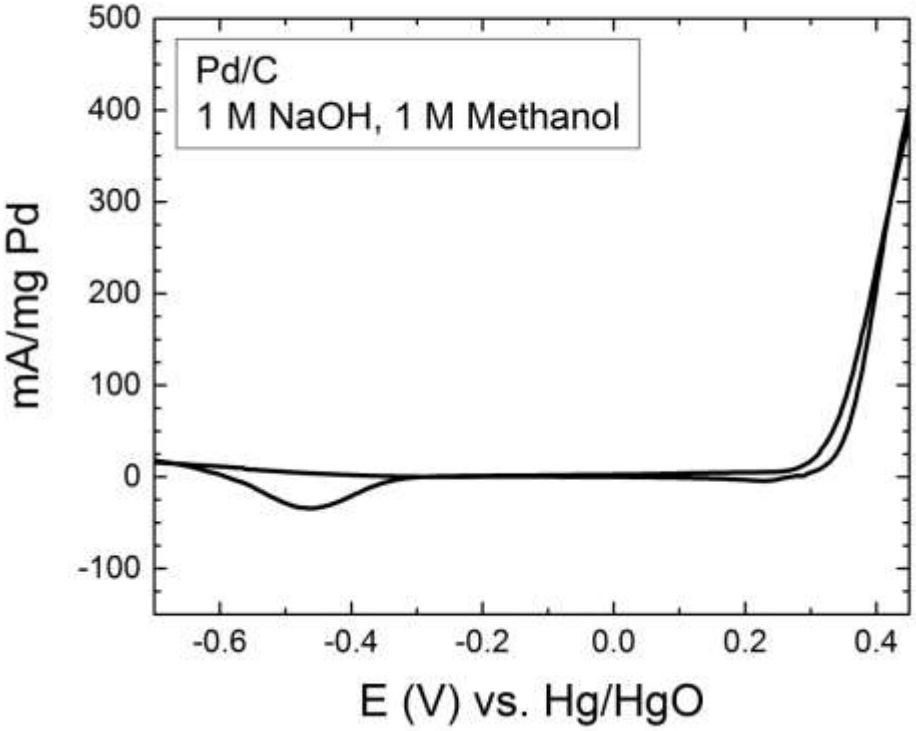

Figure S19: CVs of commercially available Pd/C in 1.0 M NaOH, 1.0 M methanol.

1. Ertem, S. P.; Tsai, T.-H.; Donahue, M. M.; Zhang, W.; Sarode, H.; Liu, Y.; Seifert, S.; Herring, A. M.; Coughlin, E. B. Photo-Cross-Linked Anion Exchange Membranes with Improved Water Management and Conductivity. *Macromolecules* **2016**, *49*, 153-161.
2. Tsai, T.-H.; Ertem, S. P.; Maes, A. M.; Seifert, S.; Herring, A. M.; Coughlin, E. B. Thermally Cross-Linked Anion Exchange Membranes from Solvent Processable Isoprene Containing Ionomers. *Macromolecules* **2015**, *48*, 655-662.
3. Terakawa, T.; Kameda, T.; Takada, S. On Easy Implementation of a Variant of the Replica Exchange with Solute Tempering in GROMACS. *J. Comput. Chem.* **2011**, *32*, 1228-1234.
4. Wright, L. B.; Walsh, T. R. Efficient Conformational Sampling of Peptides Adsorbed onto Inorganic Surfaces: Insights from a Quartz Binding Peptide. *Phys. Chem. Chem. Phys.* **2013**, *15*, 4715-4726.
5. Tang, Z.; Palafox-Hernandez, J. P.; Law, W.-C.; E. Hughes, Z.; Swihart, M. T.; Prasad, P. N.; Knecht, M. R.; Walsh, T. R. Biomolecular Recognition Principles for Bionanocombinatorics: An Integrated Approach To Elucidate Enthalpic and Entropic Factors. *ACS Nano* **2013**, *7*, 9632-9646.
6. MacKerell, A. D.; Bashford, D.; Bellott, M.; Dunbrack, R. L.; Evanseck, J. D.; Field, M. J.; Fischer, S.; Gao, J.; Guo, H.; Ha, S.; *et al*. *J. Phys. Chem. B* **1998**, *102*, 3586-3616.
7. Piana, S.; Lindorff-Larsen, K.; Shaw, David E. How Robust Are Protein Folding Simulations with Respect to Force Field Parameterization? *Biophys. J.* **2011**, *100*, L47-L49.
8. Heinz, H.; Vaia, R. A.; Farmer, B. L.; Naik, R. R. Accurate Simulation of Surfaces and Interfaces of Face-Centered Cubic Metals Using 12−6 and 9−6 Lennard-Jones Potentials. *J. Phys. Chem. C* **2008**, *112*, 17281-17290.
9. Bedford, N. M.; Hughes, Z. E.; Tang, Z.; Li, Y.; Briggs, B. D.; Ren, Y.; Swihart, M. T.; Petkov, V. G.; Naik, R. R.; Knecht, M. R.; *et al*. Sequence-Dependent Structure/Function Relationships of Catalytic Peptide-Enabled Gold Nanoparticles Generated under Ambient Synthetic Conditions. *J. Am. Chem. Soc.* **2016**, *138*, 540-548.
10. Abraham, M. J.; Murtola, T.; Schulz, R.; Páll, S.; Smith, J. C.; Hess, B.; Lindahl, E. GROMACS: High Performance Molecular Simulations through Multi-Level Parallelism from Laptops to Supercomputers. *SoftwareX* **2015**, *1–2*, 19-25.
11. Hoover, W. G. Canonical Dynamics: Equilibrium Phase-Space Distributions. *Phys. Rev. A* **1985**, *31*, 1695-1697.
12. Nosé, S. A Molecular Dynamics Method for Simulations in the Canonical Ensemble. *Mol. Phys.* **1984**, *52*, 255-268.
13. Darden, T.; York, D.; Pedersen, L. Particle Mesh Ewald: An N·log(N) Method for Ewald Sums in Large Systems. *J. Chem. Phys.* **1993**, *98*, 10089-10092.
14. Daura, X.; Gademann, K.; Jaun, B.; Seebach, D.; van Gunsteren, W. F.; Mark, A. E. Peptide Folding: When Simulation Meets Experiment. *Angew. Chem. Inter. Ed.* **1999**, *38*, 236-240.